Incommensurate phases in the two-dimensional XY model with Dzyaloshinskii-Moriya interactions

G. Albuquerque Silva,[1] J. A. Plascak,[1,2,3] and D. P. Landau[3]

[1]*Departamento de Física, Instituto de Ciências Exatas, Universidade Federal de Minas Gerais, C.P. 702, 30123-970 Belo Horizonte, MG, Brazil*

[2]*Universidade Federal da Paraíba, Centro de Ciências Exatas e da Natureza–Campus I, Departamento de Física, CCEN Cidade Universitária, 58051-970 João Pessoa, PB, Brazil*

[3]*Center for Simulational Physics, University of Georgia, Athens, Georgia 30602, USA*

(Received 2 July 2022; accepted 27 September 2022; published 13 October 2022)

The two-dimensional XY model with Dzyaloshinskii-Moriya interaction has been studied through extensive Monte Carlo simulations. A hybrid algorithm consisting of single-spin Metropolis and Swendsen-Wang cluster-spin updates has been employed. Single histogram techniques have been used to obtain the thermodynamic variables of interest and finite-size-scaling analysis has led to the phase transition behavior in the thermodynamic limit. Fluctuating boundary conditions have been utilized in order to match the incommensurability between the spin structures and the finite lattice sizes due to the Dzyaloshinskii-Moriya interaction. The effects of the fluctuating boundary conditions have been analyzed in detail in both commensurate and incommensurate cases. The Berezinskii-Kosterlitz-Thouless transition temperature has been obtained as a function of the Dzyaloshinskii-Moriya interaction and the results are in excellent agreement with the exact equation for the transition line. The spin-spin correlation function critical exponent has been computed as a function of the Dzyaloshinskii-Moriya interaction and temperature. In the incommensurate cases, optimal sizes for the finite lattices and the distribution of the boundary shift angle have been extracted. Analysis of the low temperature configurations and the corresponding vortex-antivortex pairs have also been addressed in some regions of the phase diagram.

DOI: 10.1103/PhysRevE.106.044116

I. INTRODUCTION

The two-dimensional XY model with Dzyaloshinskii-Moriya (DM) interactions has received a great deal of attention in recent years. The XY portion of the model [1] can be applied, e.g., to superfluid films [2] and Josephson junction arrays [3], and in two dimensions the model undergoes a Berezinskii-Kosterlitz-Thouless (BKT) transition characterized by an exponentially divergent correlation length and in-plane susceptibility [4–6]. On the other hand, the DM interaction part of the model [7,8], besides the original motivation for explaining weak ferromagnetism in some antiferromagnetic materials, is also responsible for some new special phenomena including, e.g., spin canting out of the CuO_2 plane in $LaCu_2O_4$ superconductors [9] and helical spin order in $Fe_xCo_{1-x}Si$ alloys [10].

The importance of the DM interaction has also been noticed in Mn monolayers, where the adjacent spins are not perfectly antiferromagneticly aligned, but slightly canted, resulting in a spin spiral structure with chiral order [11,12]. A nonzero average chirality has also been observed in Dy/Y multilayer films [13], indicating that DM interactions also exist in this material, with the chirality being ascribed to the lack of the inversion symmetry at the interfaces of the multilayer films.

The model with both XY exchange and additional DM interactions has been recently treated by Monte Carlo (MC) simulations [14]. However, it was previously shown that this more general model is, in fact, equivalent to an XY exchange renormalized Hamiltonian with the ground state having shifted angle orientation amongst the nearest-neighbor spins, with angles that are a function of the DM interaction [15]. As a result, depending on the strength of the DM interaction, incommensurability arises at low temperatures for the model. When defined on finite lattices, this leads to some spin configuration inconsistencies when using the usual periodic boundary conditions (PBC) to eliminate undesirable surface effects (in this case, besides the frustration of the spin alignments at the borders of the finite lattice, the energy of the system turns out to be significantly enhanced).

In order to circumvent the incommensurability problem on finite lattices, fluctuating boundary conditions (FBC) have been proposed [14,16]. In this way, it has been shown that FBC can in fact provide good results for the transition behavior in the cases where the incommensurability prevails. However, the role of this FBC on the system has not been studied in detail nor has the phase diagram been obtained over a wide range of the DM interaction strength.

In this work we have then revisited the two-dimensional XY model including DM interactions by employing more extensive MC simulations, making use of a hybrid algorithm consisting of single-spin updates following Metropolis algorithm and Swendsen-Wang cluster-spin updates. FBC have also been used for all lattice sizes to permit incommen-

surate structures to form, i.e., to avoid artificially imposing commensurability. We have additionally employed single histogram techniques to obtain the thermodynamic variables just above, at, and below the BKT transition temperature.

The organization of the paper is as follows. In the next section, the model and the transformation we have performed are presented. Section III is devoted to the MC simulation background and the thermodynamic variables that have been computed. In Sec. IV the results are presented and discussed and in the final section some concluding remarks are addressed. In the final section, we have also stressed that, although we have an exact transition temperature for the model as function of the DM interaction, important results concerning periodic and fluctuating boundary conditions, temperature scaling relation of the correlation length critical exponent, vortex-antivortex pair configurations, and shift angle distribution for different lattice sizes should be very useful in studying other similar systems.

II. MODEL

The Hamiltonian for the ferromagnetic XY model with DM interaction can be written as

$$\mathcal{H} = -J\sum_{\langle ij\rangle}\vec{S}_i\cdot\vec{S}_j - \vec{D}\cdot\sum_{\langle ij\rangle}(\vec{S}_i\times\vec{S}_j), \tag{1}$$

where the sums are taken over nearest-neighbor pairs of sites $\langle ij\rangle$ on a square lattice, $\vec{S}_i$ is a two-component classical vector of unit length, $J>0$ is the exchange interaction, and the DM interaction is given by the vector $\vec{D}$. By taking the DM interaction along the z axis and using the transformation proposed in Ref. [15] we get

$$\mathcal{H} = -J\sqrt{1+d^2}\sum_{\langle ij\rangle}\cos(\theta_i-\theta_j-\phi), \tag{2}$$

where $\phi = \arcsin(d/\sqrt{1+d^2})$ and we have defined $d = D/J$. Here θ_i and θ_j are the spin rotation angles of the ith and jth sites relative to the x-axis direction, respectively. The transformed Hamiltonian is thus another XY system with renormalized exchange interaction $J(d)$ and an angle phase shift $\phi(d)$, both depending on the DM interaction.

Preparing for the MC simulations, we perform an additional transformation to the above Hamiltonian, namely

$$\theta_i = \theta_i^0 - \frac{\pi}{2}(1+\sigma_i), \tag{3}$$

where σ_i takes the values ±1 and θ_i^0 denotes a trial angle at the site i. If $\sigma_i=-1$, θ_i just keeps the same value; if $\sigma_i=1$, it means that θ_i is rotated by an angle of π. Combining Eqs. (2) and (3) we arrive at an Ising-type Hamiltonian

$$\mathcal{H} = -\sum_{ij}J_{ij}\sigma_i\sigma_j, \tag{4}$$

where

$$J_{ij} = J\sqrt{1+d^2}\cos\left(\theta_i^0-\theta_j^0-\phi\right) \tag{5}$$

is an effective nonuniform Ising coupling between spins. This transformation turns out to be very useful for implementing the Swendsen-Wang cluster-spin portion of the algorithm to the model.

III. MONTE CARLO SIMULATIONS AND THERMODYNAMIC VARIABLES

A. Monte Carlo simulations

We use a hybrid Monte Carlo algorithm, which combines the standard single-spin Metropolis update [17] and the Swendsen-Wang cluster-spin update [18]. In the single-spin update, a new random orientation for the spin $\vec{S}_i$ is chosen at each site i and, if it lowers the energy, the new state is accepted; otherwise, it is accepted only with a probability according to the standard Metropolis criterion.

In order to reduce the critical slowing down of this simulation, the Swendsen-Wang (SW) cluster algorithm is also used. In an initial spin configuration of Hamiltonian (4) we choose $\sigma_i=1$ for all the sites. If $J_{ij}>0$ in (5), we put a bond between ith and jth sites with a probability $P(J_{ij}) = 1-\exp(-2J_{ij}/k_BT)$, where k_B is the Boltzmann constant and T the temperature. If $J_{ij}<0$, no bond is inserted. After clusters are constructed by putting bonds between spins, every cluster has the same possibility either to rotate by an angle of π or just to keep the same value. In general, one SW sweep related to Eqs. (3) and (4) followed after one Metropolis sweep related to Eq. (2).

As reported in Ref. [14], depending on the value of d, incommensurability emerges between the spin orientations and the finiteness of the lattice, preventing the normal use of periodic boundary conditions (PBC). This can be seen by computing the phase shift Δ across the boundaries (same row or column) of a lattice size L, which can be given by

$$\Delta = L\phi \text{ (a)}, \quad \Delta = 2n\pi \text{ (b)}, \quad L = 2n\pi/\phi \text{ (c)}, \tag{6}$$

where n is a positive nonzero integer. Whenever Eq. (6b) holds, the structure is commensurate with the lattice and the use of periodic boundary conditions will be suitable for the finite system. Otherwise, the structure is incommensurate with the lattice. Nevertheless, one can look for *optimal* lattice sizes by considering values of L close to the result obtained by using Eq. (6c) for different integers n.

However, as will be discussed in the next section, the incommensurability problem can be more efficiently circumvented by adopting fluctuating boundary conditions [16]. It can be done as follows. Suppose there is a phase shift Δ across the boundary at the same row and column, i.e., $\Delta = \theta_{1,y}-\theta_{L,y}$ and $\Delta = \theta_{x,1}-\theta_{x,L}$ for $1\leqslant x\leqslant L$ and $1\leqslant y\leqslant L$, in such a way that Eq. (6b) is not satisfied. After a hybrid MC sweep to update the spins while fixing Δ, one employs an extra, standard Metropolis sweep to update Δ while fixing all the spins. It has been shown that employing this FBC is better than the usual PBC when the system is incommensurate [14]. In this case, one hybrid MC step is composed by combining one Metropolis sweep, one SW sweep, and one Metropolis sweep updating just the boundary phase shift. Although one can use PBC whenever the phase shift and lattice size turn out to be commensurate, a detailed comparison between both boundary conditions are still necessary in this case.

The MC simulations have been performed on $L\times L$ square lattices, with total sites $N=L^2$ and L ranging from $L=8$ to $L=128$. Typically, 10^5-10^6 MC data points have been discarded for equilibration and $10^8-3\times10^8$ MC data points have been retained for constructing the single histograms.

The sampling interval for collecting data has been 10 hybrid MC sweeps for all lattice sizes, making the total length of the simulations ten times longer than the numbers specified above. For instance, for the largest simulated lattice $L = 128$ a total of more than 3×10^9 configurations have been generated for the construction of the histograms.

B. Thermodynamic variables

The data that have been collected from the simulations consisted basically of the energy, magnetization, and the phase shifts across the boundaries. Derived quantities such as cumulants and fluctuations could also be easily obtained. However, due to the spin rotation along both the x and y directions at low temperatures (when the strength of DM interaction is not very small), the usual magnetization, which is the regular order parameter in the two-dimensional XY model [19,20], does not play the role of an order parameter in the present system. This is because of the periodic and oscillating spin arrangement that results when the DM interaction is included. Nevertheless, according to the spin arrangement in the ground state, we can define a different, and more convenient, order parameter as follows:

$$m = \frac{1}{L^2}\sqrt{M_x^2 + M_y^2},$$
$$M_x = \sum_{i=1}^{L^2} \cos[\theta_i + (x_i + y_i)\phi],$$
$$M_y = \sum_{i=1}^{L^2} \sin[\theta_i + (x_i + y_i)\phi], \tag{7}$$

where (x_i, y_i) is the coordinate of the ith spin and $x_i, y_i \in [1, L]$. Thus $m = 1$ in the ground state and, for finite lattices, should decrease as the temperature increases.

According to the finite-size-scaling theory [19,21,22] of the BKT critical behavior, the above quantity, for all temperatures T below T_c, where T_c is the BKT transition temperature, should have a power-law scaling behavior of the type

$$m \propto L^{-x}, \tag{8}$$

$T \leqslant T_c$, with a temperature dependent exponent x, and no such power-law behavior for temperatures $T > T_c$. Exactly at the transition temperature $T = T_c$ the exponent x is equal to $\eta/2$ [19], where $\eta = 1/4$ is the corresponding spin-spin correlation function critical exponent. These exponents decrease as the temperature decreases and go towards zero in the $T \to 0$ limit. Thus we can extract information about the transition, in the thermodynamic limit, by analyzing the behavior of m for different lattice sizes.

Another useful quantity is the fourth-order cumulant of the order parameter, originally suggested by Binder to analyze the Ising model critical properties [23]. In the present case we have considered the reduced form of the cumulant that can be written as

$$U_4 = 1 - \langle m^4\rangle/3\langle m^2\rangle^2, \tag{9}$$

where the angle bracket denotes a thermal average. Binder has shown that, for large enough lattices, there is a *fixed point* in the U_4 curves that is independent on the system size L and the location of this fixed point gives the transition point. So, the Binder cumulants are scale independent at the critical point and can also be used to determine the phase transition temperature T_c. For an XY model we expect that the fourth-order cumulants will become equal below the BKT transition temperature; however, corrections to finite-size scaling are sometimes still present in the cumulant crossings for the lattice sizes at hand. When these finite-size effects happen, and when the crossings have a systematic shift with L, we can extrapolate the transition temperature to the thermodynamic limit by fitting the corresponding data to [6,14,22]

$$T_{\text{cross}} = T_c + B/(\ln L)^2, \tag{10}$$

where T_{cross} is the temperature of the cumulant crossings and B a nonuniversal constant. A derivation of the above equation using a renormalization group approach can be found in Ref. [6] and more explicitly in Refs. [24,25].

IV. RESULTS

A. BKT transition temperature

The crossings of the reduced form of the cumulants (9) have been used to compute the BKT transition temperature T_c for several values of the DM interaction d. This is a very convenient quantity because we do not need *a priori* knowledge of any exponent, even when one has to use Eq. (10). We have thus studied the pure XY model with $d = 0$ for two main reasons: first, in order to compare our transition temperature with previous estimates from the literature and, second, because this transition temperature, as we will see in the next subsection, is needed to get the exact transition line as a function of the DM interaction.

The top panel in Fig. 1 shows the magnetization fourth-order cumulant U_4 as a function of the temperature T, for different values of the lattice size L. Note that here, and also in what follows, all temperatures are given in units of J/k_B. The lines in Fig. 1 have been obtained from single histogram reweighting of data taken at different temperatures T_0 for each lattice, with T_0 within the interval $0.91 < T_0 < 0.94$. We note that the larger the lattice size the more MCS had to be discarded (consequently, even more MCS had to be taken for the averages) in order to get reliable estimates of U_4. In doing so, for the larger lattices we have always tested the energy probability distribution at the crossing points (which were different from the temperature where the histograms were taken) to ensure that its wings do not suffer from large statistical uncertainties. It is apparent from the top panel of Fig. 1 that the cumulant crossings are still quite dependent on the lattice sizes. However, taking as reference the minimum size $L_{\text{min}} = 8$, there is a clear systematic decrease in the temperature crossing T_{cross} as the other sizes increase from $L > 8$, making the use of Eq. (10) quite suitable in this case. Although it cannot be clearly seen in Fig. 1, the same qualitative crossings happen when the minimum lattice sizes $L_{\text{min}} = 16$ and $L_{\text{min}} = 24$.

In fact, we would expect the cumulants to all be the same for temperatures lower than the crossing points, since the transition should always be present for any $T < T_{\text{BKT}}$. For instance, in the bottom panel of Fig. 1 we have the magnetization cumulants for the larger lattices and lower temperatures.

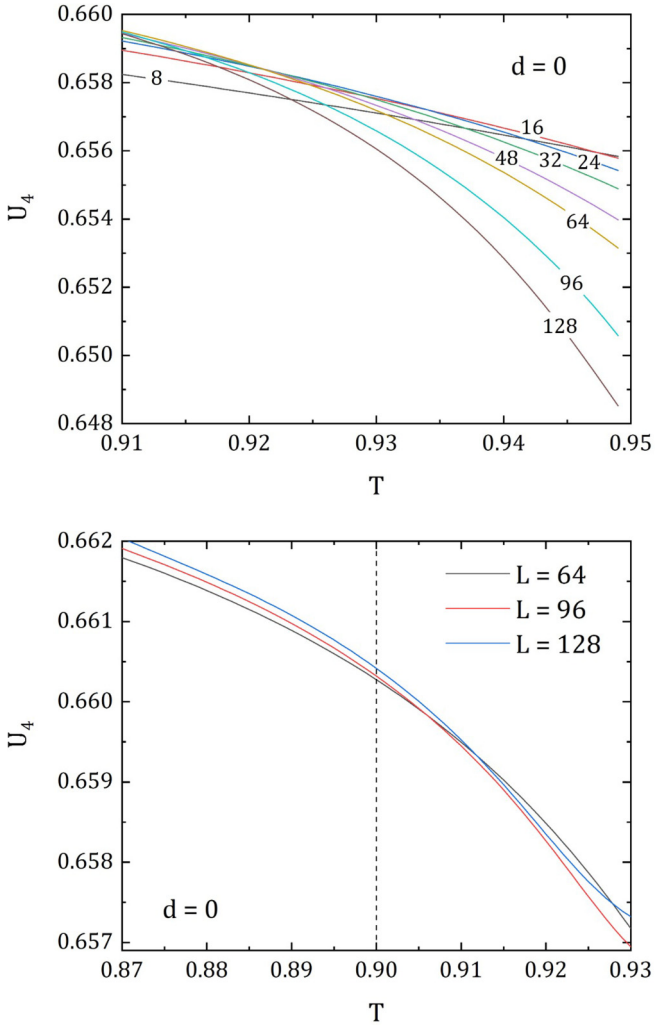

FIG. 1. Binder cumulant U_4 of the order parameter vs temperature T for different lattice sizes for the XY model, $d = 0$, using PBC. The data points, with corresponding error bars, have been omitted for clarity. In the bottom panel only the larger lattices have been considered with new data taken at $T = 0.9$ (dashed line) and analyzed with single histograms.

While the cumulants still cross for $L = 64$ and $L = 96$ (as we will see below, this crossing value is actually compatible with the extrapolated evaluation of the BKT transition temperature), the cumulants for $L = 96$ and $L = 128$ seem to be almost parallel in this region of temperature, a fact that can signal a possible BKT transition. For this reason, we can consider the crossing temperatures as an indication of the BKT transition T_c.

The temperatures of the cumulant crossings $T_{\text{cross}}(L, L_{\text{min}})$ are obtained from the data of the top panel of Fig. 1, taken as reference the cumulants for $L_{\text{min}} = 8, L_{\text{min}} = 16$, and $L_{\text{min}} = 24$. The results are shown in Fig. 2 as a function of $(\ln L)^{-2}$. The error bars of the crossings have been estimated as described in the Appendix. It is interesting to note, in all cases, the strong size dependence of the data, with the scaling regime, as predicted by Eq. (10), being only achieved for the lattice sizes greater than $L \geqslant L_s$, with the smallest size $L_s = 64$.

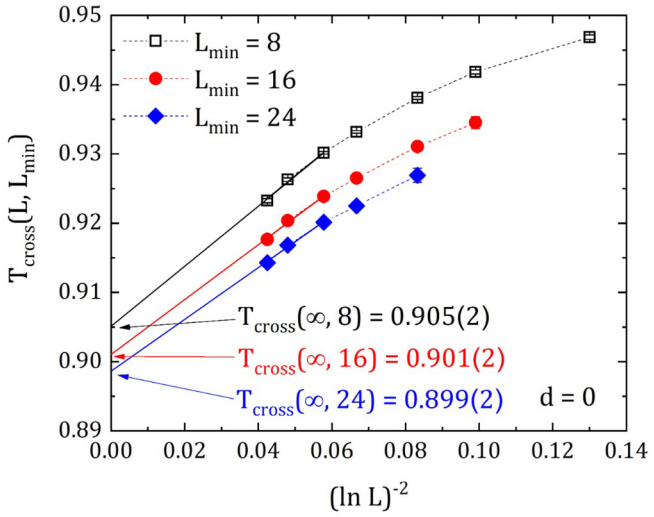

FIG. 2. Temperature of the crossings of the Binder cumulant of the order parameter $T_{\text{cross}}(L, L_{\text{min}})$ as a function of different reference lattice sizes L_{min} when $d = 0$ (XY model) using PBC. The upper, middle, and lower sets of data points correspond to crossings with $L_{\text{min}} = 8$, $L_{\text{min}} = 16$, and $L_{\text{min}} = 24$, respectively. The dashed lines are just guides to the eye, while the solid lines are linear fits using Eq. (10) for lattice sizes $L \geqslant 64$. The extrapolated transition temperatures in the $L \to \infty$ limit, $T_c(\infty, L_{\text{min}})$, are indicated by the arrows.

In addition, we can see that the $L \to \infty$ limit from each linear fit, $T_c(\infty, L_{\text{min}})$, still depends on the reference lattice size L_{min}. For this reason, we can further assume that $T_{\text{cross}}(\infty, L_{\text{min}})$ should follow the same scaling behavior given by Eq. (10). The result is shown in Fig. 3, from which, with an additional fit, leads to $T_c(\infty, \infty) = T_c = 0.894(1)$, a value that compares very well to $T_c = 0.8935(1)$ and

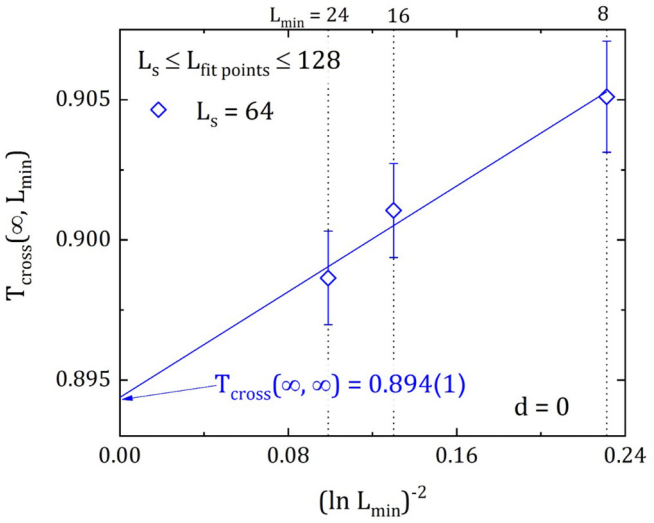

FIG. 3. Temperature of the extrapolated crossings of the Binder cumulant of the order parameter $T_{\text{cross}}(\infty, L_{\text{min}})$ as a function of different reference lattice sizes L_{min} (shown on top of the figure) when $d = 0$ (XY model) using PBC. The vertical dashed lines locate the reference lattice sizes L_{min} and the solid line is a linear fit using Eq. (10). L_s is the smallest lattice size considered in the fits of Fig. 2. The extrapolated transition temperature is indicated by the arrow.

TABLE I. BKT transition temperature $T_c(d)$ and the ratio $T_c(d)/\sqrt{1+d^2}$ for some values of the DM interaction d. In the last column we have some results from the literature. The last line gives the average of $\overline{T_c(d)/\sqrt{1+d^2}} \equiv \overline{T}(0)$ for all values of d (including $d \to \infty$).

d	$T_c(d)$	$T_c(d)/\sqrt{1+d^2}$	$T_c(d)$ (literature)
0	0.894(1)	0.894(1)	0.8935(1) [26]
			0.8935(5) [27]
0.05	0.902(1)	0.901(1)	
0.25	0.930(2)	0.902(2)	
0.5	0.997(3)	0.892(3)	1.013(4) [14]
0.75	1.120(1)	0.896(1)	
1	1.268(2)	0.897(1)	1.292(6) [14]
1.25	1.4491(2)	0.9053(1)	
1.5	1.6203(4)	0.8988(2)	
$d \to \infty$		0.897(1)	
	$\overline{T}(0)$	0.898(4)	

$T_c = 0.8935(5)$ obtained in Refs. [26] and [27], respectively. These values are also listed in Table I where $T_c \equiv T_c(0)$.

Following the same procedure as above we can compute the transition temperature for other values of the DM interaction. As an example, Figs. 4 show the results for $d = 0.5$ using FBC and $d = 1$ using PBC. Since for $d = 1$ we have $\phi = \pi/4$, according to Eq. (6 c), the finite lattices must be multiples of 8 in order to keep the commensurability with the spin configurations, hence allowing use of PBC. As for the case of the pure XY model, $d = 0$, we can see that the scaling regime in these two examples has been only reached for the largest lattices. In fact, this is the general trend for all values $d > 0$.

The results of $T_c(\infty, L_{\min})$ from Fig. 4, as a function of $(\ln L_{\min})^{-2}$, are shown in Fig. 5. The additional extrapolation can still improve the estimate of the BKT temperature T_c slightly.

Table I gives the BKT transition temperature $T_c(d)$ so obtained for some additional values of the DM interaction

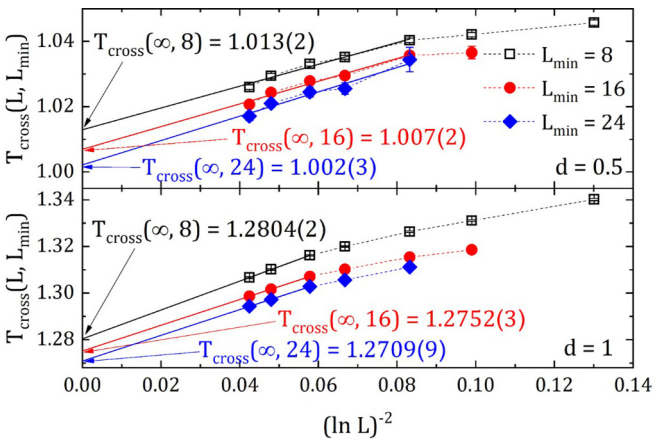

FIG. 4. Same as Fig. 2 for $d = 0.5$ using FBC (upper panel) and $d = 1$ using PBC (lower panel). The extrapolated transition temperatures are also indicated in the figures for the three reference lattice sizes.

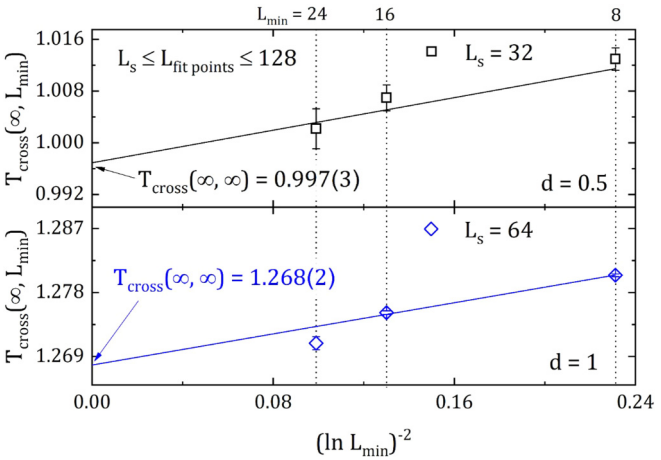

FIG. 5. Same as Fig. 3 for $d = 0.5$ using FBC (upper panel) and $d = 1$ using PBC (lower panel). L_s is the smallest lattice size considered in the fits. The extrapolated transition temperatures are also indicated for the three reference lattice sizes.

d together with some available values previously obtained from the literature [14,26,27]. Note that the transition temperatures for $d = 0.5$ and $d = 1$ are comparable to the previous estimates from Ref. [14]. However, the present ones are expected to be more accurate due to the greater statistics obtained from the simulations. We also note that the BKT transition temperatures from Ref. [14] are higher than the present ones. This is a consequence of the results in [14] being obtained using all lattice sizes and, accordingly, resulting in a smaller slope for the data extrapolation.

In Table I we also find the transition temperature for a smaller value of d namely $d = 0.05$, in order to seek whether the transition temperature starts first decreasing as d increases from zero before having a positive slope for higher values of d, as has been reported in Refs. [28,29] for the square and triangular lattices, respectively. We can see that the present result for $d = 0.05$ indeed increases and $T_c(d)$ has a monotonic behavior for larger values of the DM interaction. The decreased value of T_c for small d obtained in Refs. [28,29] could be related to the use of PBC instead of FBC, as in our approach. The expected behavior of the transition temperature as d increases will be better elucidated in the following subsection.

B. Transition temperature as a function of the DM interaction

The corresponding phase diagram of the model in the DM interaction d versus the BKT transition temperature $T_c(d)$ plane, using the values from Table I, is shown in the upper inset of Fig. 6. Note that as $d \to \infty$ the shift angle goes to $\phi \to \pi/2$ and the transition frontier becomes a straight line. Thus, taking Eq. (2) and considering $\phi = \pi/2$, we can perform an extra simulation to obtain an effective transition temperature $T_{\text{eff}} = T_c(d)/d$. This result gives, in fact, the asymptotic slope of the transition line as $d \to \infty$. Interestingly enough, the result is, within the error bars, the same as the transition temperature of the pure XY model (see Table I).

To better understand this behavior, and motivated by the definition of the order parameter in Eq. (7), we consider the

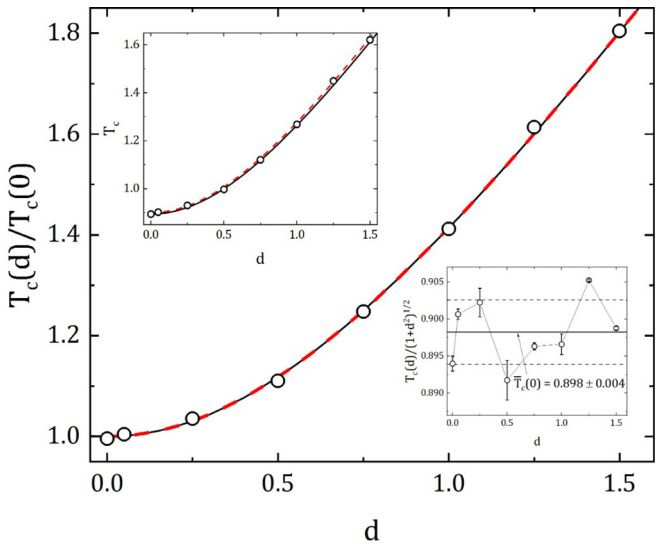

FIG. 6. *Main curve.* Phase diagram in the DM interaction d versus the reduced transition temperature $T_c(d)/T_c(0)$ plane. The circles are the results from Table I with $T_c(0) = 0.898(4)$. The solid line is the function $\sqrt{1+d^2}$ and the dashed line a fit with $\sqrt{r+d^2}$ with r given in the text (both lines are almost coincident to each other in the scale of the figure). *Upper inset.* $T_c(d)$ versus d where the solid line comes from Eq. (13) with $T_c(0) = 0.894(1)$ and the dashed line is the hyperbola using Eq. (14) with the parameters in the text. *Bottom inset.* Values of $T_c(d)/\sqrt{1+d^2}$ from the third column in Table I as a function of d. The solid line locates the mean value and the dashed lines the error bars.

following Hamiltonian:

$$\mathcal{H} = -J(d) \sum_{\langle ij \rangle} \cos[\tilde{\theta}_i(d) - \tilde{\theta}_j(d)], \tag{11}$$

where

$$\begin{aligned} \tilde{\theta}_i(d) &= \theta_i - (x_i + y_i)\phi(d), \\ \tilde{\theta}_j(d) &= \theta_j - (x_j + y_j)\phi(d). \end{aligned} \tag{12}$$

Since j is a nearest neighbor of i, one has always $(x_i + y_i) - (x_j + y_j) = 1$ and $\tilde{\theta}_i(d) - \tilde{\theta}_j(d) = \theta_i - \theta_j - \phi(d)$. This means that Hamiltonian (11) above is equivalent to Hamiltonian (2). From (11) the transition temperature is thus given by

$$T_c(d) = T_c(0)\sqrt{1+d^2}. \tag{13}$$

The above equation gives the exact transition line of the XY model with DM interaction. It is the equation of a hyperbola, which is symmetric regarding d, as it should be. This is the same result previously obtained for the one-dimensional version of the model [15].

From the above equation, it is also clear that the ratio $T_c(d)/\sqrt{1+d^2}$ is a constant, equivalent to the BKT transition of the pure model. The third column on Table I and the corresponding data in the bottom inset in Fig. 6 show this trend. The mean value $\overline{T}(0) = 0.898(4)$ is also quite comparable to the $T_c(0)$ obtained in the previous subsection and from values in the literature.

On the other hand, the ratio $T_c(d)/T_c(0) = \sqrt{1+d^2}$ is the equation of a rectangular hyperbola with equal semiaxis. Figure 6 also shows $T_c(d)/T_c(0)$, with $T_c(0) = \overline{T}(0) = 0.898(4)$, plotted together with the function $\sqrt{1+d^2}$ (solid line) and a fit with $\sqrt{r+d^2}$, where r is a fitting parameter (dashed line). In both cases one gets a quite nice agreement with the simulations and the value $r = 1.000(2)$ very close to the expected value $r = 1$.

The solid line in the upper inset of Fig. 6 is obtained from Eq. (13) with $T_c(0) = 0.894(1)$ and the dashed line is a fit of the simulation results with the hyperbole function

$$T_c(d) = T^*\sqrt{r+d^2}, \tag{14}$$

where T^* and r are the fitting parameters. Again, in both cases, a good agreement has been achieved with the simulation results, and the fitting parameters $T^* = 0.906(4)$ and $r = 0.99(1)$ are also comparable to the expected ones.

C. BKT transition and critical exponent η for $T < T_c$

We expect the transition, for any value of d, to remain of BKT type for temperatures $T < T_c$, since the transformed Hamiltonian (2) is, in essence, just another XY model with renormalized exchange interaction (although, as we shall see below in Sec. IV D, the low temperature spin configurations seem to have lower symmetry than that of the two-dimensional XY model and, as a consequence, misleadingly suggest a conventional phase transition). For the particular example of the pure model shown in the top panel of Fig. 1, one can see that the lattice sizes are still a little too small to fully reflect this behavior, because the cumulants are not all the same for temperatures lower than the crossing points. This is shown more clearly in the bottom panel of Fig. 1. This same tendency is also seen for other values of the DM interaction. For this reason, in order to confirm the BKT transition at lower temperatures we have studied the order parameter m, defined in Eq. (7), in conjunction with its scaling behavior (8). As an example, we have chosen the value $d = 0.5$ with FBC, and the results of the log-log plot of m, as a function of the lattice size L, are shown in Fig. 7 for different temperatures, slightly above and below T_c. For lower temperatures, in this case for $T \lessapprox 1.0$, all the data are along straight lines whose slopes decrease as T decreases. For higher temperatures, the behavior of m starts to deviate from straight lines signifying that the scaling regime of Eq. (8) is no longer valid and the system has been driven above the BKT transition. The wider dashed line in Fig. 7 represents the threshold of the transition exponent $\eta = 1/4$.

From the slopes of the data in Fig. 7 (and some additional ones not shown in that figure for still lower temperatures), we can compute the corresponding spin-spin correlation function critical exponent η. The results, so obtained, are shown in Fig. 8 as a function of the temperature T. It is clear from this figure that the transition is indeed of BKT type and the exponent $\eta \to 0$ as the temperature $T \to 0$, as expected. Some selected values of the exponents of Fig. 8 are displayed in Table II. Although there are some oscillations in the η values as the temperature is changed close to $T \approx 1$, we can roughly estimate the BKT transition temperature as $T_c = 1.009(9)$, a

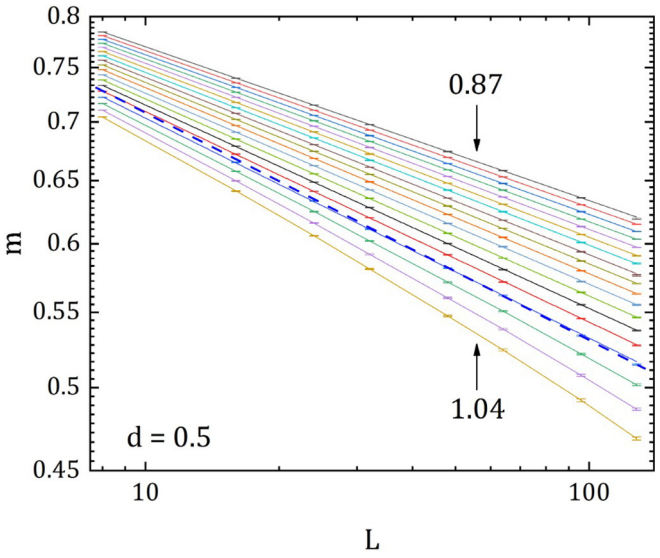

FIG. 7. Log-log plot of the order parameter m as a function of the lattice size L for different values of the temperature T for $d = 0.5$. From the lower temperature 0.87 to the higher temperature 1.04, all the steps are 0.01. The results come from histogram reweighting of data taken at temperatures $T = 0.9$, 0.97, and 1. The wider dashed straight line corresponds to the slope that gives $\eta = 1/4$. The lines for $T \leqslant 1$ are linear fits to the data, while for $T > 1$ they are just guides to the eyes.

value which is quite consistent with the transition temperature $T_c = 0.997(3)$ given in Table I. The results are similar for other values of the DM interaction d.

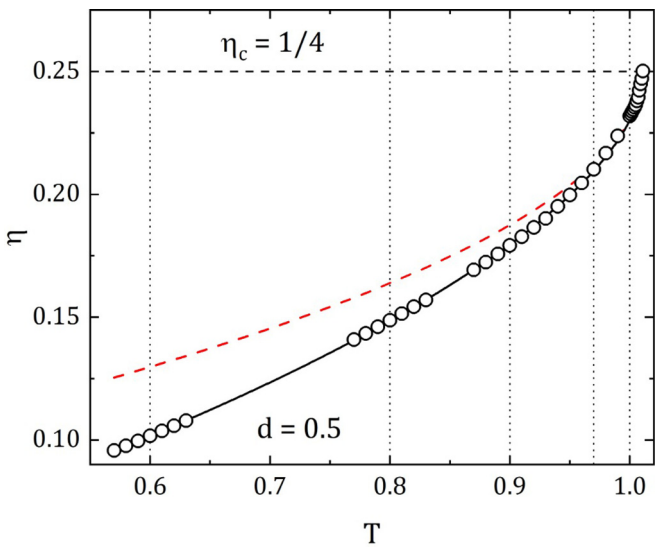

FIG. 8. Spin-spin correlation function critical exponent η as a function of the temperature T for $d = 0.5$. The vertical dotted lines locate the temperature at which the data were taken for constructing the histograms and the horizontal dotted line is the threshold of the critical exponent $\eta_c = 1/4$. The full line is a fit according to Eq. (15) with the parameters given in the text. The dashed line is a fit with only the two first terms of Eq. (15) and considering only data for $T > 0.97$.

TABLE II. Spin-spin correlation function critical exponent η for some values of temperature T for $d = 0.5$.

T	η	T	η
1.012	0.2516(9)	0.88	0.1724(2)
1.011	0.2502(9)	0.87	0.1692(2)
1.01	0.2486(9)	0.83	0.1570(2)
1.009	0.2498(9)	0.82	0.1542(2)
1	0.2318(4)	0.81	0.1514(2)
0.99	0.2238(4)	0.8	0.1488(2)
0.98	0.2168(4)	0.79	0.1460(2)
0.97	0.2102(2)	0.78	0.1434(2)
0.96	0.2046(2)	0.77	0.1408(2)
0.95	0.1996(2)	0.63	0.1068(2)
0.94	0.1952(4)	0.62	0.1058(2)
0.93	0.1902(2)	0.61	0.1038(2)
0.92	0.1866(2)	0.6	0.1016(2)
0.91	0.1828(2)	0.59	0.0996(2)
0.9	0.1792(2)	0.58	0.0976(2)
0.89	0.1756(4)	0.57	0.0956(2)

The data in Fig. 8 can be further analyzed by considering a temperature dependence of η as

$$\eta(T) = \frac{1}{4} - C\left(1 - \frac{T}{T_c}\right)^{1/2} + C'\left(1 - \frac{T}{T_c}\right) + C''\left(1 - \frac{T}{T_c}\right)^{3/2}, \quad (15)$$

where C, C', and C'' are fitting parameters and we use $T_c = 1.011$. The first two terms in (15) come from Refs. [30,31], where close to the transition temperature T_c the leading behavior is expected to have a square-root singularity. A fit with only those two terms, close to the transition point [fitting the data for $T > 0.97$ with $C = 0.189(3)$ and extrapolating to $T < 0.97$], is shown by the dashed line in Fig. 8. Although a good agreement has been obtained close to T_c, the fitted curve is far from the simulation results in an extended region of lower temperatures. On the other hand, by considering higher order contributions, as explicitly given in Eq. (15), one can see a quite good agreement, in the entire temperature range, with fit parameters $C = 0.179(3)$, $C' = -0.12(1)$, and $C'' = 0.06(1)$ (shown by the solid line in Fig. 8). In addition, with these parameters we have $\eta(0) = 0.01(1)$ and the slope at $T = 0$ $d\eta(T)/dT|_{T\to 0} = 0.12(2)$, which should be compared to the exact $\eta(0) = 0$ and $d\eta(T)/dT|_{T\to 0} = 1/2\pi = 0.169\ldots$ from the spin-wave phase [30,31].

D. Low temperature phase configurations

It is interesting to see the topology of the spin arrangements as the present BKT transition is passed through. As discussed above, at zero temperature the system orders with neighboring spins having shift angles ϕ. However, as the temperature increases, there are fluctuations in these neighboring orientations. Figure 9 depicts the corresponding spin configuration for $d = 0.5$ with FBC and lattice size $L = 48$ at three different values of temperature. In the top panels we show the spin configurations and in the bottom panels respective color

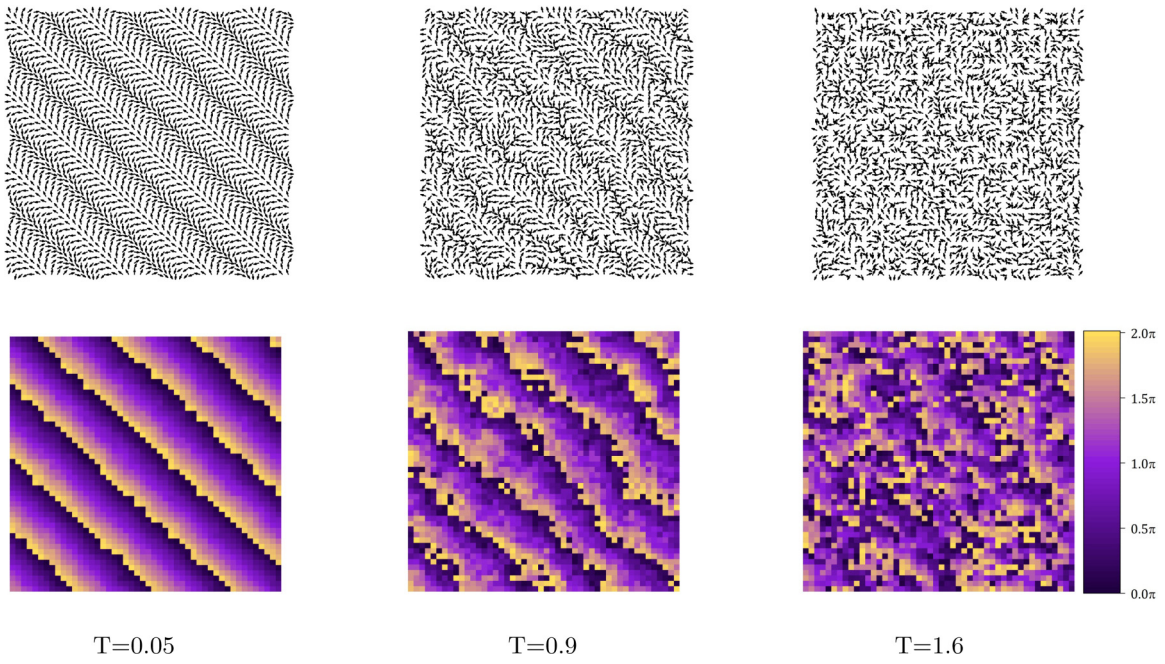

FIG. 9. Typical spin configurations given by the arrows (top panels) and color gradient of the spin orientation angle in radians (bottom panels) for $d = 0.5$ and lattice size $L = 48$ with FBC. Low temperature in the two left panels, just below the BKT transition temperature in the two middle panels, and high temperature in the two right panels.

gradients for the spin angle in radians. The striped ordering of the spins is, perhaps, better seen in the color gradient structure of the bottom panels: at low temperatures (left panels) the order is well defined; just below the BKT transition temperature (middle panels) the order still persists with larger fluctuations; and, eventually, the disordered state is achieved for higher temperatures (as depicted in the right panels).

The strip arrangement, due to the DM interaction, in some sense seems to cover up the topological structure of vortices in these systems and one might falsely expect that the incommensurate chiral order leads to a phase transition to a lower symmetry phase than that of the two-dimensional XY model and hence to a conventional phase transition. However, this is indeed not the case, because we can invert the spins by the angle ϕ and obtain similar configurations of the pure XY model. As an example, Fig. 10 shows the spin configurations, together with the location of the vortex-antivortex pairs, for $d = 0.5$. The top panels correspond to a temperature just below the transition temperature and the bottom panels to a temperature above the transition. The left panels show the actual configurations and the right panels the configurations with reverted spins. The dots and stars locate the vortex-antivortex cores. We can see that the vortex-antivortex pairs are still present even in the actual configuration of the spins due to the DM interaction.

E. FBC versus PBC and incommensurate shift angle distribution

For DM interactions where the lattice sizes become incommensurate with the spin orientations, the FBC have provided more reliable results than the usual PBC. Although in the previous results for $d = 0.5$ the FBC have been implemented in the same finite lattices used with PBC for commensurate values of d, one can as well investigate the behavior for the *optimal* sizes using Eq. (6c). For instance, for $d = 0.5$ we have $\phi = 0.4636\ldots$ rad and $L = 13.5516\ldots$, meaning that one can choose $L = 14, 28, 42, \ldots$ instead of multiples of

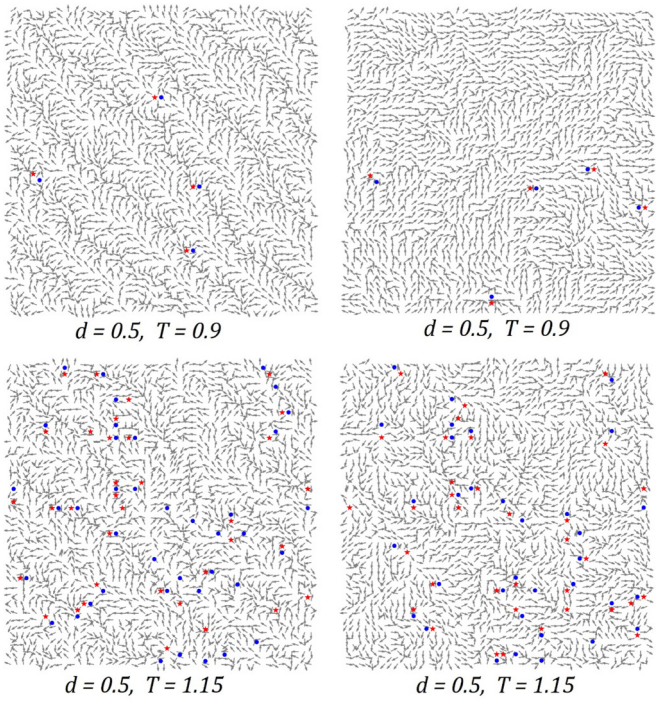

FIG. 10. Spin configurations for $d = 0.5$, just below the transition temperature in the top panels and just above the transition temperature in the bottom panels. The left panels show the actual configurations and the right panels the configurations with reverted spins. The dots and stars locate the vortex-antivortex pairs.

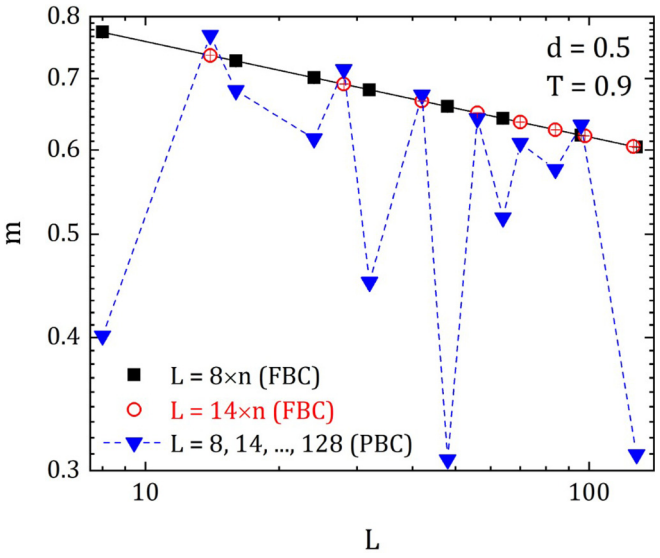

FIG. 11. Log-log plot of the order parameter m as a function of the lattice size L for $d = 0.5$ and $T = 0.9$. The squares correspond to lattice sizes that are multiples of 8 with $n \leqslant 16$, while the circles are optimal sizes which are multiples of 14 with $n \leqslant 9$. The triangles are data obtained by considering all lattices with PBC. The solid line is a fit to the scaling function given by Eq. (8) using only the results obtained from FBC. The dashed line is just a guide to the eyes.

$L = 8$ as before. Figure 11 depicts the log-log plot of the order parameter m as a function of lattice sizes L considering both choices. With the data obtained from FBC, the critical exponent is given by $\eta = 0.08954(4)$ and is comparable to the value $\eta = 0.0896(1)$ obtained by using only lattice sizes that are multiples of 8. It is then clear that, as soon as one uses FBC, the sizes of lattices are not so important for getting the transition properties of the model.

Figure 11 also shows the results for all considered lattices using PBC. We can clearly see that most of the values fall either far below or above the fit obtained using FBC. It is also interesting that even for the "optimal" lattice sizes, with PBC, the results are still rather far from the fit obtained by using FBC.

It should be stressed here that, as in the Ising model [32], different types of boundary conditions influence the universal value of the fourth-order cumulant U_4^* in the thermodynamic limit (although the transition temperature is not affected by them). In this case, for $d = 0$, we estimate $U_4^* = 0.6599(3)$ with PBC and $U_4^* = 0.6468(1)$ with FBC.

The use of optimal lattice sizes with FBC in the incommensurate case has an important effect on the probability distribution of the shift angle Δ that results from the simulation.

The behavior of such probability distributions (which, to our knowledge, has not been previously reported in the literature) should be quite useful when treating other incommensurate systems. Figure 12 show the shift angle probability distribution $P^*(\Delta) = P(\Delta)/P(\langle\Delta\rangle)$ for several values of temperature T for $d = 0.5$ and two different lattice sizes, namely $L = 48$ and $L = 41$. In order to have a better visualization, in each case the actual probability $P(\Delta)$ has been divided by the computed probability $P(\langle\Delta\rangle)$ at the mean value $\langle\Delta\rangle$,

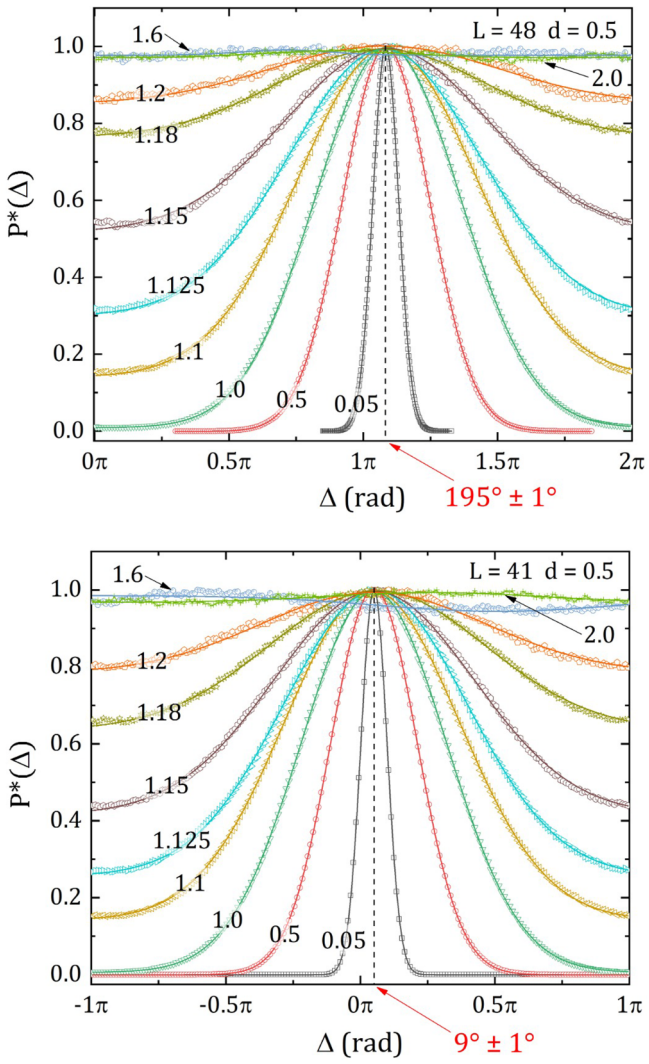

FIG. 12. Shift angle distribution $P^*(\Delta)$ as a function of Δ for $d = 0.5$ and several values of temperature. The lattice size is $L = 48$ in the upper panel and $L = 41$ in the bottom panel. The lines are Gaussian fits according to Eq. (16). The arrows indicate the mean value of the shift angle in degrees.

so one always has $P^*(\langle\Delta\rangle) = 1$. In general, all the $P^*(\Delta)$ distributions are Gaussian and have been fitted using

$$P^*(\Delta) = P_0 + A\, e^{-\frac{(\Delta-\langle\Delta\rangle)^2}{2w^2}}, \tag{16}$$

where P_0 and A are constants and w is the width of the distribution. We can see that the width w decreases as T decreases. On the other hand, as the temperature increases above the BKT temperature, the distribution flattens and reaches a constant value, meaning that in this region the phase shift is not so important due to the strong thermal fluctuations. We can clearly see that the only difference between the optimal size [here $L = 41$ obtained from Eq. (6c) with $n = 3$] and any other size will be just the mean value of the shift angle Δ, which for optimal lattice sizes will be closer to zero. It should also be stressed that if we consider FBC for commensurate lattices we obtain the same qualitative behavior above described with $\langle\Delta\rangle \approx 0$.

V. CONCLUDING REMARKS

The two-dimensional XY model with Dzyaloshinskii-Moriya (DM) interaction has been studied through extensive Monte Carlo simulations by employing a hybrid algorithm consisting of single-spin Metropolis updates and Swendsen-Wang cluster-spin updates. Single histogram reweighting techniques have been introduced to obtain the thermodynamic variables close to the Berezinskii-Kosterlitz-Thouless (BKT) transition and finite-size scaling has been used to analyze the phase transition behavior in the thermodynamic limit. Fluctuating boundary conditions (FBC) have been utilized in order to match the incommensurability between the spin structure and the finite lattice sizes due to the DM interaction. The effects of the FBC have been analyzed in detail and the BKT transition temperature, as well as the corresponding spin-spin correlation function critical exponent, has been obtained as a function of the DM interaction and temperature.

It is clear that the transition is indeed of BKT type for any value of the DM interaction, and the critical exponent η decreases from $1/4$ towards zero as the temperature decreases. The ground state is composed of strips of aligned spins that lose their conformation as the temperature approaches the BKT transition temperature.

In incommensurate cases, optimal sizes for the finite lattices, or any other lattice sizes, furnish coherent results as soon as FBC are considered. The distribution of the boundary shift angle, however, has mean values closer to zero for optimal lattices and quite different values for other sizes.

Another important result in the present work is the analytic equation for the transition temperature of the model as a function of the DM interaction, which has been verified by simulation. Besides the fact that this relation could be used in the study of quantum versions of the XY system with DM interaction, there are some important features of the present simulations that helped lead to a better understanding of the physical behavior of the model. In addition, some of these features should certainly be quite useful in studying models with other types of anisotropies, for instance, as follows.

(i) The importance of considering fluctuating boundary conditions, even to compute the exponent η, as depicted in Fig. 11.

(ii) The scaling behavior of the exponent η as a function of temperature, given by Eq. (15), which extends to the entire temperature range.

(iii) Looking at the spin configurations of Fig. 9, it is not at all obvious that the model still exhibits vortex and antivortex pairs and a BKT transition. It looks, indeed, at first sight like a conventional transition. However, we have shown that the vortices and antivortices are still present and the transition is really of BKT type.

(iv) The Gaussian distribution of the shift angle in Figs. 12 is expected to be the same for other models.

ACKNOWLEDGMENTS

This research was supported by CNPq, CAPES, and FAPEMIG (Brazilian agencies). We thank A. R. Bergeron for fruitful discussions concerning the initial simulations on this model. This study was also supported in part by resources and technical expertise from the Georgia Advanced Computing Resource Center (GACRC), a partnership between the University of Georgia's Office of the Vice President for Research and Office of the Vice President for Information Technology. We would also like to acknowledge Professor G. Weber for the invaluable assistance in the use of the Statistical Mechanics Computer Lab facilities at UFMG.

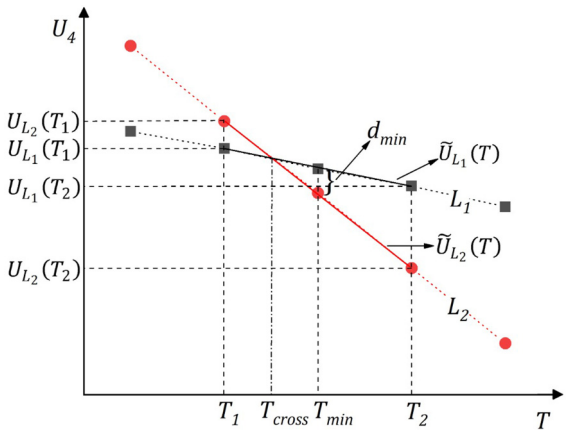

FIG. 13. Sketch of the estimate of the cumulant crossing between two diffferent lattice sizes L_1 (squares) and L_2 (circles). $d_{\min}$ is the minimum value of the magnitude of the difference of the cumulants $|U_{L2} - U_{L_1}|$ at $T_{\min}$, from which one locates neighboring temperatures T_1 and T_2. $\tilde{U}_{L_1}(T)$ is the straight line equation (full line) through points $[T_1, U_{L_1}(T_1)]$ and $[T_2, U_{L_1}(T_2)]$, while $\tilde{U}_{L_2}(T)$ is the corresponding straight line equation through points $[T_1, U_{L_2}(T_1)]$ and $[T_2, U_{L_2}(T_2)]$. T_{cross} is the temperature where the lines $\tilde{U}_{L_1}(T)$ and $\tilde{U}_{L_2}(T)$ meet.

APPENDIX

This Appendix briefly describes the method used to compute the crossing temperatures from the cumulants as well as the estimate of the corresponding errors.

Figure 13 sketches typical results for the cumulants U_{L_1} and U_{L_2} of two different lattice sizes L_1 and L_2 as a function of temperature. If $d_{\min}$ is the minimum value of the magnitude of the difference of the cumulants $|U_{L_2} - U_{L_1}|$ occurring at $T_{\min}$, we can determine its two neighboring temperatures T_1 and T_2, as shown in Fig. 13. From these points we construct the equations of straight lines $\tilde{U}_{L_1}(T)$ and $\tilde{U}_{L_2}(T)$, which meet at T_{cross} where $\tilde{U}_{L_1}(T_{\text{cross}}) = \tilde{U}_{L_2}(T_{\text{cross}})$, leading to

$$T_{\text{cross}} = T_2 - \frac{\Delta U_{T_2}}{\Delta U_{T_2} - \Delta U_{T_1}} \Delta T_{12}, \tag{A1}$$

where

$$\begin{aligned} \Delta T_{12} &= T_2 - T_1, \\ \Delta U_{T_1} &= U_{L_2}(T_1) - U_{L_1}(T_1), \\ \Delta U_{T_2} &= U_{L_2}(T_2) - U_{L_1}(T_2). \end{aligned} \tag{A2}$$

Since T_1, T_2, and ΔT_{12} are fixed in a particular data set, the error in crossing temperature δT_{cross} comes basically from the simulations and the histogram reweighting on the other quantities appearing in Eqs. (A1) and (A2), in this case the

corresponding cumulants at different temperatures. Accordingly, one has [33]

$$\delta T_{\text{cross}} = \sqrt{\sum_{i=1}^{2}\sum_{j=1}^{2}\left[\frac{\partial T_{\text{cross}}}{\partial U_{L_i}(T_j)}\right]^2 [\delta U_{L_i}(T_j)]^2}, \tag{A3}$$

where the partial derivatives are taken from Eqs. (A1) and (A2) and $\delta U_{L_i}(T_j)$ is the uncertainty coming from the simulation data.

A more compact form of the above expression can be given by

$$\delta T_{\text{cross}} = 2C\Delta T, \tag{A4}$$

where ΔT is the chosen resolution of the temperature interval where the histograms are taken (in our case $\Delta T = 0.001$) and C specifies the contributions from the cumulants and their uncertainties for the lattice sizes L_1 and L_2 at temperatures T_1 and T_2. More explicitly, one has

$$C = \frac{\sqrt{C_1 + C_2}}{\left(\Delta U_{T_2} - \Delta U_{T_1}\right)^2}, \tag{A5}$$

with

$$\begin{aligned} C_1 &= \left\{\left[\delta U_{L_1}(T_1)\right]^2 + \left[\delta U_{L_2}(T_1)\right]^2\right\}(\Delta U_{T_2})^2, \\ C_1 &= \left\{\left[\delta U_{L_1}(T_2)\right]^2 + \left[\delta U_{L_2}(T_2)\right]^2\right\}(\Delta U_{T_1})^2. \end{aligned} \tag{A6}$$

Estimates of the error of the cumulants at different temperatures are obtained by dividing the data into bins and computing the cumulants for each bin using the respective histograms. It is then possible to estimate the mean value and the error of the cumulants at any temperature.

[1] T. Matsubara and H. Matsuda, Prog. Theor. Phys. **16**, 569 (1956).
[2] T. Ohta and D. Jasnow, Phys. Rev. B **20**, 139 (1979).
[3] D. J. Resnick, J. C. Garland, J. T. Boyd, S. Shoemaker, and R. S. Newrock, Phys. Rev. Lett. **47**, 1542 (1981).
[4] V. L. Berezinskii, Sov. Phys. JETP **32**, 493 (1971).
[5] J. M. Kosterlitz and D. J. Thouless, J. Phys. C: Solid State Phys. **6**, 1181 (1973).
[6] J. M. Kosterlitz, J. Phys. C: Solid State Phys. **7**, 1046 (1974).
[7] I. Dzyaloshinsky, J. Phys. Chem. Solids **4**, 241 (1958).
[8] T. Moriya, Phys. Rev. Lett. **4**, 228 (1960); Phys. Rev. **120**, 91 (1960).
[9] D. Coffey, K. S. Bedell, and S. A. Trugman, Phys. Rev. B **42**, 6509 (1990).
[10] M. Uchida, Y. Onose, Y. Matsui *et al.*, Science **311**, 359 (2006).
[11] M. Bode, M. Heide, K. V. Bergmann *et al.*, Nature **447**, 190 (2007).
[12] P. Ferriani, K. von Bergmann, E. Y. Vedmedenko, S. Heinze, M. Bode, M. Heide, G. Bihlmayer, S. Blugel, and R. Wiesendanger, Phys. Rev. Lett. **101**, 027201 (2008).
[13] S. V. Grigoriev, Yu. O. Chetverikov, D. Lott, and A. Schreyer, Phys. Rev. Lett. **100**, 197203 (2008).
[14] H. Liu, J. A. Plascak, and D. P. Landau, Phys. Rev. E **97**, 052118 (2018).
[15] F. C. Alcaraz and W. F. Wreszinski, J. Stat. Phys. **58**, 45 (1990).
[16] P. Olsson, Phys. Rev. Lett. **73**, 3339 (1994).
[17] N. Metropolis, A. W. Rosenbluth, M. N. Rosenbluth *et al.*, J. Chem. Phys. **21**, 1087 (1953).
[18] R. H. Swendsen and J. S. Wang, Phys. Rev. Lett. **58**, 86 (1987).
[19] M. S. S. Challa and D. P. Landau, Phys. Rev. B **33**, 437 (1986).
[20] E. Rastelli, S. Regina, and A. Tassi, Phys. Rev. B **69**, 174407 (2004); **70**, 174447 (2004).
[21] M. E. Fisher, in *Proceeding of the International Summer School "Enrico Fermi" 1970, Course 51, Varenna, Italy*, edited by M. S. Green (Academic Press, New York, 1971).
[22] D. P. Landau and K. Binder, *A Guide to Monte Carlo Simulation in Statistical Physics*, 5th ed. (Cambridge University Press, Cambridge, UK, 2021).
[23] K. Binder, Z. Phys. B: Condens. Matt. **43**, 119 (1981).
[24] S. T. Bramwell and P. C. W. Holdsworth, J. Phys.: Condens. Matter **5**, L53 (1993).
[25] D. Venus, Phys. Rev. B **105**, 235440 (2022).
[26] Y.-D. Hsieh, Y.-J. Kao, and A. W. Sandvik, J. Stat. Mech. (2013) P09001.
[27] P. H. Nguyen and M. Boninsegni, Appl. Sci. **11**, 4931 (2021).
[28] S. Yun-Zhou, L. Hui-Ping, and Y. Lin, Commun. Theor. Phys. (Beijing, China) **46**, 663 (2006).
[29] Y.-Z. Sun, L. Yi, and J.-S. Wang, Commun. Comput. Phys. **11**, 1169 (2012).
[30] J. M. Kosterlitz and D. J. Thouless, in *Progress in Low Temperature Physics*, edited by D. F. Brewer (Elsevier, Amsterdam, 1978), Chap. 5.
[31] R. Gupta and C. F. Baillie, Phys. Rev. B **45**, 2883 (1992).
[32] W. Selke, Eur. Phys. J. B **51**, 223 (2006).
[33] Evaluation of measurement data—Guide to the expression of uncertainty in measurement, https://www.bipm.org/documents/20126/2071204/JCGM_100_2008_E.pdf/cb0ef43f-baa5-11cf-3f85-4dcd86f77bd6.